

# Projected distances to host galaxy reduce SNIa dispersion

R. Hill,<sup>1,2</sup> H. Shariff,<sup>1,3</sup> R. Trotta,<sup>1,3,4\*</sup> S. Ali-Khan,<sup>1</sup> X. Jiao,<sup>3,5</sup> W. Parker,<sup>1,6</sup>  
M. Paulus,<sup>1,7</sup> D.A. van Dyk,<sup>1,3,4</sup>, L.B. Lucy<sup>1</sup>

<sup>1</sup>*Astrophysics Group, Physics Department, Imperial College London, Prince Consort Rd, London SW7 2AZ*

<sup>2</sup>*Department of Physics and Astronomy, the University of British Columbia, 6244 Agricultural Road, Vancouver, BC, V6T 1Z1*

<sup>3</sup>*Imperial Centre for Inference and Cosmology, Astrophysics Group, Blackett Laboratory, Prince Consort Rd, London SW7 2AZ*

<sup>4</sup>*Data Science Institute, William Penney Laboratory, Imperial College London, London SW7 2AZ*

<sup>5</sup>*Statistics Section, Mathematics Department, Huxley Building, South Kensington Campus, Imperial College London, London SW7 2AZ*

<sup>6</sup>*Bay House school & Sixth Form, Gomer lane, Gosport, Hampshire, PO12 2QP*

<sup>7</sup>*Department of Physics and Astronomy, University of Glasgow, Glasgow G12 8QQ*

Accepted XXX. Received YYY; in original form ZZZ

## ABSTRACT

We use multi-band imagery data from the Sloan Digital Sky Survey (SDSS) to measure projected distances of 280 supernova type Ia (SNIa) from the centre of their host galaxies, normalized to the galaxy’s brightness scale length. We test the hypothesis that SNIas further away from the centre of their host galaxy are less subject to dust contamination (as the dust column density in their environment is smaller) and/or come from a more homogeneous environment. We find a statistically significant difference (at the 5% significance level) in the observed colour correction distribution between SNIas that are near and those that are far the centre of their host. We estimate the residual scatter of the two subgroups to be  $0.074 \pm 0.021$  for the far SNIas, compared to  $0.106 \pm 0.009$  for the near SNIas – an improvement of 30%, albeit with a low statistical significance of  $1.4\sigma$ . This confirms the importance of host galaxy properties in correctly interpreting SNIa observations for cosmological inference.

**Key words:** keyword1 – keyword2 – keyword3

## 1 INTRODUCTION

The Nobel Prize for Physics 2011 was awarded for the discovery that the universe was accelerating. [Riess et al. \(1998\)](#) and [Perlmutter et al. \(1999\)](#) used SNIas as standardizable candles to infer the existence of an additional component in the energy density of the universe, now called dark energy. The number of SNIa observations since that seminal discovery has grown rapidly: we now have hundreds of spectroscopically confirmed SNIas (e.g., [Astier et al. 2006](#); [Wood-Vasey et al. 2007](#); [Amanullah et al. 2010](#); [Kowalski et al. 2008](#); [Kessler et al. 2009](#); [Freedman et al. 2009](#); [Contreras et al. 2010](#); [Balland et al. 2009](#); [Bailey et al. 2008](#); [Hicken et al. 2009](#); [Suzuki et al. 2012](#); [Rest et al. 2014](#); [Betoule et al. 2014a](#)), which have been used to measure the distance modulus to  $z \sim 1.8$ . This low-redshift probe of the expansion history of the Universe, coupled with the high-redshift measurements of the Cosmic Microwave Background anisotropies, has been a vital tool for determining the equation of state of dark energy, and to put constraints on modified gravity models.

SNIas are a subclass of supernovae defined by the absence of H lines in their spectra and the presence of Si lines. The generally accepted understanding of a SNIa explosion is that of a CO white dwarf accreting material from a companion star. The gravitational pressure ignites a runaway thermonuclear reaction that leads to the catastrophic unbinding of the white dwarf. While this scenario is generally agreed upon in literature, the details of their formation, including the nature of the progenitor, as well as the exact explosion mechanism remain unclear. The diversity of SNIas appears however to suggest that SNIas are produced by more than one progenitor channel: no single channel (i.e. single degenerate scenario, where a CO white dwarf accretes mass from a non-degenerate companion star; or double degenerate scenario, the merging of two white dwarves) can account for all of the available observations (see e.g. [Maeda & Terada \(2016\)](#) for a recent review).

Given the emerging support for the idea that the diversity in SNIas observations can only be explained by postulating multiple sub-classes (perhaps even within the ‘normal’ SNIa type), it becomes even more important to clarify any links between the SNIas variability and their galactic environment. Much work has thus been expended in studying the influence of the SNIa galactic environment onto its

\* E-mail: r.trotta@imperial.ac.uk

observable properties – in particular, possible residual dependencies of the brightness and/or colour of the SNIa after the empirical standardization corrections have been applied.

Empirical corrections are applied by linearly adjusting the SNIa's  $B$ -band peak magnitude for stretch (Phillips 1993; Phillips et al. 1999) (slow declining SNIas are brighter) and colour excess (Riess et al. 1996; Jha et al. 2007) (bluer SNIas are brighter). After such corrections, the residual scatter around the Hubble diagram is reduced to  $\sim 0.1$  mag, which is what enables the use of SNIas as cosmological probes.

Since the standardization procedure is empirical (although partially justified by theoretical models, e.g. Kasen & Woosley (2007)), much effort has gone into trying to establish whether the residual scatter can be further reduced by including other observable proxies of the SNIa's environment and/or progenitor channel. These include host galaxy mass, star formation rate, metallicity (e.g. Lampeitl et al. (2010); Sullivan et al. (2010)), stellar population age, spectral lines width, host morphology and location within the host. For a recent review of environmental correlations, see Anderson et al. (2015a).

There is general agreement that SNIas in more massive galaxies are (post corrections) brighter (Kelly et al. 2010; Sullivan et al. 2006, 2010; Campbell et al. 2015; Shariff et al. 2016), although estimates of the difference range from  $0.055 \pm 0.022$  mag (Shariff et al. 2016) to  $0.11$  mag (Sullivan et al. 2010). This effect could be a reflection of the hosts' metallicity (Gallagher et al. 2008), given the well-known mass-metallicity correlation in early-type galaxies. Several studies have investigated the influence of galaxy morphology and/or star formation rate (SFR), reporting that SNIas with a smaller stretch parameter (i.e., rapid decliners) occur more often in lenticular/elliptical galaxies (Henne et al. 2017) as well as in passive galaxies (Lampeitl et al. 2010). Lampeitl et al. (2010) found evidence that galaxies with lower star formation rates produce, on average, dimmer SNIas. D'Andrea et al. (2011) analysed host-galaxy spectra to obtain metallicity and star-formation rates from a subset of the SNSS-II SNIas. They discovered that SNIas from high metallicity host galaxies are  $\sim 0.1$  mag brighter. Additionally they found a  $> 3\sigma$  correlation between specific star formation rate and Hubble residuals. However, no significant correlation has been found between the SNIas' colour and the hosts' morphology or SFR. For example, Campbell et al. (2013) used a sample of 581 photometric SNIas and applied a series of host galaxy corrections to the Hubble distance including metallicity, mass, star formation rate, specific star formation rate and age of galaxies. They found a  $> 5\sigma$  significant reduction in the Hubble residuals when host galaxy mass was added as an additional covariate. However, the improvement was less significant for the other covariates. More recently, much work has focused on evaluating the residual effect of the local SFR at the site of the explosion, with somewhat contradictory results (Anderson et al. 2015b; Rigault et al. 2013; Kelly et al. 2015; Jones et al. 2015).

Establishing the dependence (if any) of the SNIas inferred luminosity on environmental effects is important both in terms of potentially improving SNIas as standard candles and in order to reduce any remaining systematic effects. For example, Kelly et al. (2015) demonstrated that SNIas in regions of high UV flux have a smaller residual dispersion. Fur-

thermore, reducing the remaining intrinsic dispersion below  $0.1$  mag would enable measuring spatial weak lensing correlations between SNIas, a new probe of cosmological parameters (Scovaccicchi et al. 2016).

With this in mind, the goal of this paper is to revisit the question of the influence of the projected radial position of the SNIa within its host, but using a larger sample of SNIas and a more sophisticated statistical analysis than was previously available.

In this work we extend and improve previous (null) results by Ivanov et al. (2000); Yasuda & Fukugita (2010); Galbany et al. (2012), who analyzed SNIas samples containing between 62 to 195 objects. Ivanov et al. (2000) used a sample of 62 SNIas and found no evidence of correlation between stretch or colour corrections and deprojected galactocentric distances from the hosts. They also separated the SNIa sample according to galactic morphology, again finding no effect. Yasuda & Fukugita (2010) looked at the first year SDSS-II SN sample (137 SNIas at  $0.05 \leq z \leq 0.3$ ) and considered possible correlations of colour  $c = E(B - V)$  with galactocentric distance, without finding any significant correlation. More recently, Galbany et al. (2012) performed a similar analysis on a larger sample containing 195 SNIas and again did not find an effect.

One of the motivations for the above studies was to investigate the effect (if any) of the radial metallicity gradient in the galaxy on the SNIa's properties. By selecting a sub-group at high projected galactocentric radius, one might hope to select a more homogeneous metallicity environment, and hence a more homogeneous sub-class of SNIa progenitors. Furthermore, the effect of dust and extinction within the host also changes with galactocentric distance. The confounding effect of dust along the line of sight is a well-known source of uncertainty (and potentially systematic errors) in the empirical correction procedure. Indeed there is evidence that the conventional linear colour correction is inadequate, in that it fails to distinguish between intrinsic colour variations in the SNIas and host galaxy dust effects (Mandel et al. 2016). This is one of the reasons of the current effort to obtain light curve in the rest-frame Near Infrared – a wavelength range much less affected by dust (Mandel et al. 2009).

However, given the high observational cost of obtaining NIR lightcurves for a sample at cosmological distances, it would be interesting to determine whether the location of the SNIa explosion within the host can help select SNIas that are less affected by dust. This could lead to a higher precision (by using SNIas with lower residual scatter) and accuracy (by removing or mitigating a potential source of systematic error).

Higher extinction is expected in regions with a higher star formation rate, and particularly in more central regions of star-forming galaxies. Hence, SNIas at small galactocentric radii are expected to be redder, an effect that could be due to the local ISM but also to the progenitor's rings of dust, particularly for active, late-type galaxies. Indeed, Anderson et al. (2015b) showed that redder SNIa events are found more centrally in a sample of star-forming galaxies. They used the equivalent width of the unresolved sodium doublet (NaD) to quantify the amount of extinction along the line of sight, finding that SNIas with NaD detections (indicating high absorption) are much more likely to be cen-

trally located within their hosts. Largely removing the effect of reddening due to the ISM might help in identifying intrinsic colour variations in the SNIas and/or the reddening due to Circumstellar Material (CSM). Therefore, our aim is to investigate whether segregating the SNIa sample into sub-groups according to their projected radial distance from the host can help in selecting a sub-group (at large galactocentric radii) that is less affected by dust and more homogeneous in its post-correction magnitude. Indeed, [Lira \(1996\)](#) predicted that low reddened SNIas would have very little interstellar gas and dust. This could be either due to the distance from host or the galaxy type ([Sternberg et al. 2011](#)). As forcibly argued by [Mandel et al. \(2016\)](#), the empirical corrections to the observed magnitude currently implemented in the popular *SALT2* fitter might introduce biases in the measured distances, for they bundle together intrinsic colour variations with extrinsic (i.e., due to host dust) variations, especially so at both extremes of the colour range. If it were possible to identify a sub-group of SNIas that are less affected by extrinsic colour variations, this would be a useful tool to access their intrinsic colour variability and use such measurements as cross checks of systematics due to inappropriate statistical modeling of the type pointed out by [Mandel et al. \(2016\)](#).

In this paper, we increase the sample size significantly with respect to previous work, to 280 SNIas (a sub-set of the 368 SDSS SNIas in JLA); we re-fit galaxy images from scratch (for consistency) and adopt a more sophisticated (and powerful) statistical approach for the estimation of the residual scatter after empirical corrections.

This paper is structured as follows. In Section 2 we discuss details of the modeling of the brightness profile of the host galaxies, how we estimate the SNIas' galactocentric distance to their host, as well as how we split the SNIas into two groups based on this quantity. In Section 3 we briefly summarize *BAHAMAS*, the Bayesian parameter inference procedure we adopt to estimate the residual scatter in the two sub-groups of SNIas. We present our results in Section 4 and conclude in Section 5.

## 2 HOST GALAXY MODELLING AND FITTING

### 2.1 Data

We investigate the 368 SNIas from the Sloan Digital Sky Survey (SDSS) II Supernova Survey ([Sako et al. 2014](#)) contained in the Joint Light-curve Analysis (JLA) SNIa compilation ([Betoule et al. 2014b](#)), spanning the redshift range  $0.01 \leq z \leq 1.30$  and with median redshift  $z_{\text{med}} = 0.23$ . We require estimates of the *SALT2* ([Guy et al. 2007](#)) parameters of each SNIa, namely the peak B-band magnitude,  $m_B$ , the lightcurve stretch correction,  $x_1$ , and colour correction,  $c$ . For these quantities we adopt the estimates obtained by [Betoule et al. \(2014b\)](#).

We obtain the necessary imaging to identify the position of each SNIa in its host galaxy from the SDSS Data Release 10 (DR10) ([Ahn et al. 2014](#)). Images of  $100 \times 100$  pixels were acquired, centred on the right ascension and declination of each host galaxy, as identified by the SDSS-II Supernova Survey. Given the pixel size of the SDSS, this resulted in

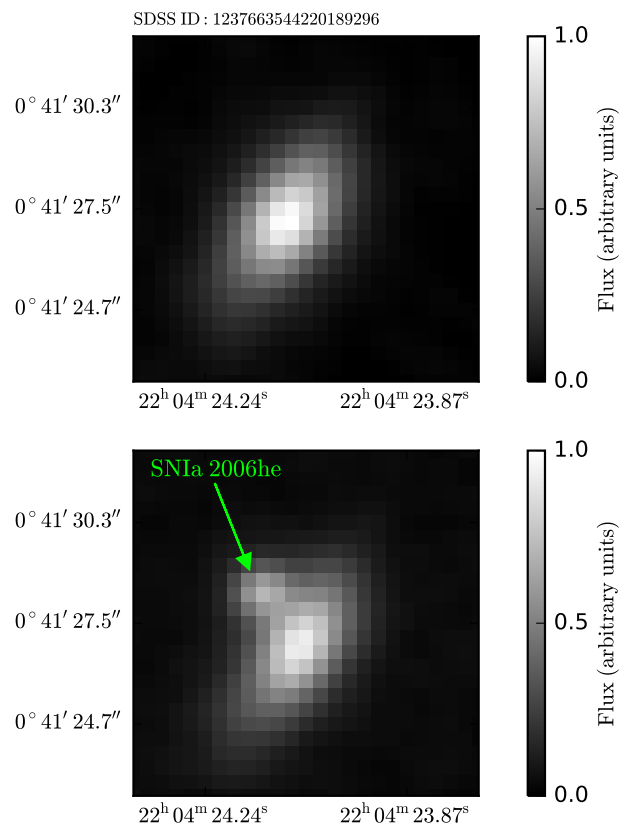


**Figure 1.** Top: a typical galaxy image after stacking and smoothing. The image was produced by adding the 5 filters, *ugriz*, available in the SDSS DR10, convolving with a Gaussian filter with standard deviation equal to one pixel and normalizing the result to one. (The gray scale is thus arbitrary.) Bottom: image of the corresponding SNIa taken from the SDSS-II Supernova Survey. The SNIa ID in this case is 2006he, and the corresponding host galaxy ID is 1237663544220189296. The SNIa images were not used to fit galaxy intensity profiles, but only serve as illustrative examples.

square images of approximately 396 arcsec sides. Galaxies are observed in five filters, *ugriz* ([Doi et al. 2010](#)). We stack the images with equal weights and normalise them to obtain co-added galaxy images, with arbitrary flux units.

With increasing redshift of the galaxies, each of the bands is measuring bluer restframe wavelengths, and therefore the apparent size of the galaxy might increase in a given band. The simple co-adding of all the five bands attempts to mitigate against this effect. A more sophisticated approach would involve re-weighting each band with a weight determined as a function of the galaxy's redshift. However, [Galbany et al. \(2012\)](#) did not find that this effect had an appreciable impact on their result (when using *r* band photometry only), and therefore we neglect it in the present study. We convolve each image with a Gaussian filter with standard deviation of one pixel in each direction. This helps reduce noise without blending small galaxies into the background. An example of a galaxy image resulting from this procedure is shown in Fig. 1.

## 2.2 Galaxy Images Fitting

Our aim is to obtain approximate isophotes for the host galaxies and use these as a simple proxy for their dust column density. We are interested in determining the scale length of the galaxy, i.e., the projected distance to the point of the galaxy at which the luminosity drops to a specified fraction of its value at the centre. The scale length then gives the characteristic scale by which to measure the projected distance (i.e., galactocentric distance) of the SNIa.

Because obtaining an estimate of the scale length does not require sophisticated models for the light emission from the galaxy, we model each galaxy's radial intensity profile,  $I(r)$ , with a simple elliptical function (Sérsic 1963), which follows an exponential law,

$$I(r) = I_e \exp \left( -b_n \left[ \left( \frac{r}{r_e} \right)^{1/n} - 1 \right] \right), \quad (1)$$

where  $r_e$  is the scale length,  $I_e$  is the intensity of the galaxy at  $r_e$ ,  $n$  is the Sérsic index (which controls the drop-off in intensity from the centre), and  $b_n$  is the solution to the transcendental equation,

$$\Gamma(2n) = 2\gamma(2n, b_n). \quad (2)$$

Here,  $\Gamma(x)$  is the gamma function and  $\gamma(x, a)$  is the incomplete gamma function. We use the polynomial approximations of the solution to Eq. (2) given in MacArthur et al. (2003) for  $n \leq 0.36$  and Ciotti & Bertin (1999) for  $n > 0.36$ . At the distance from the centre of the galaxy equal to the scale length  $r_e$ , the central intensity has dropped by a factor  $e^{-b_n}$ . The mean value of  $b_n$  for our sample of galaxies is  $\bar{b}_n = 1.3$ , which corresponds to a drop in brightness of  $\approx 30\%$ .

The origin of the pixel coordinate system that we use for each galaxy image coincides by construction with the galaxy centre as reported in the SDSS-II Supernova Survey (Sako et al. 2014). However, for internal consistency we refit the centre of the galaxy, parameterizing it by its pixel coordinates  $(x_0, y_0)$ . Furthermore, we allow for elliptical isophotes with free ellipticity parameter,  $\epsilon$ , and orientation angle,  $\phi$  (measured counter-clockwise from the  $y$ -axis of the image to the semi-major axis of the ellipse). With this, the radial distance  $r$  in Eq. (1) of a pixel with coordinates  $(x, y)$ , is given by

$$r(x, y) = \left( x_p^2 + \frac{y_p^2}{q^2} \right)^{1/2}, \quad (3)$$

where

$$x_p = (x - x_0) \cos(\theta) + (y - y_0) \sin(\theta), \quad (4)$$

$$y_p = -(x - x_0) \sin(\theta) + (y - y_0) \cos(\theta), \quad (5)$$

$q = 1 - \epsilon$ , and  $\theta = \phi + \frac{\pi}{2}$ .

Our model of the intensity profile of each host galaxy thus includes seven free parameters, namely  $\Theta = \{x_0, y_0, \phi, \epsilon, I_e, r_e, n\}$ . The likelihood function is calculated at each observed pixel intensity,  $\mu_{ij} \equiv D(x_i, y_j)$ , as an independent Gaussian, and summed over all pixels in the image. The mean of the Gaussian for pixel  $(x_i, y_j)$  is the measured intensity,  $\mu_{ij}$ , and its standard deviation is  $\sigma_{ij} \equiv \sqrt{\mu_{ij}}$  (using the high-count Gaussian approximation to the underly-

ing Poisson distribution for each pixel). Thus the likelihood is, up to an irrelevant normalization constant:

$$-2 \ln \mathcal{L}(\Theta) = \sum_{i,j} \frac{[I(r(x_i, y_j)|\Theta) - \mu_{ij}]^2}{\mu_{ij}}, \quad (6)$$

where  $I(r(x_i, y_j))$  is the predicted intensity at pixel  $(x_i, y_j)$  from the model with parameters  $\Theta$ . (Note that unit-wise Eq. (6) is valid as our images have been scaled and are thus unitless.). The Maximum Likelihood Estimate (MLE) of  $\Theta$  was obtained using a differential evolution scheme implemented in the astronomical image fitting software *IMFIT*. (For details on *IMFIT* and the corresponding differential evolution maximization technique see Erwin (2015).) Images are cropped to a size of  $50 \times 50$  pixels for larger galaxies and  $25 \times 25$  pixels for smaller galaxies (about 25% and 75%, respectively) before computing the MLEs. This ensures that possible background contaminants are removed from the image without cutting out any of the galaxy's light. Each fit is then visually inspected to ensure that the fitted luminosity profile is a good description of the co-added image by checking the overlay of the image with isophotes contours obtained from the *IMFIT* fit at  $0.5r_e$ ,  $1r_e$ ,  $1.5r_e$ ,  $2r_e$  and  $2.5r_e$ . We also compared our best-fit galaxy centre values with the host galaxy coordinates given by Sako et al. (2014): the median displacement is 0.59 pixels. A fit was deemed "successful" if (i) the iso-brightness contours followed the general shape of the galaxy, with  $r_e$  being located somewhere in the vicinity of the outer edge of the galaxy; (ii) if  $(x_0, y_0)$  was in the visual centre of the galaxy and compared well with the host galaxy coordinates in Sako et al. (2014) and (iii) the residuals were close to 0 throughout the model image. An example of a successful fit is shown in Fig. 2.

Some fits are unsuccessful because of insufficient image quality. In some cases the galaxy is found in a region of significantly higher noise and in other cases the galaxy is too faint. Both of these effects lead to a host intensity within a few percent of the background. An example of each of these cases is shown in Fig. 3. SNIas associated with a host galaxy that could not be fit are removed from the sample. Of the 368 host galaxy images, 88 cannot be successfully fit, leaving a sample of 280 SNIas for our analysis.

## 2.3 Sub-groups of SNIas based on galactocentric distance to host

From our best-fit parameters we compute the projected distance of the SNIa from its host galaxy with Eq. (3):

$$r_{\text{SN}} = r(x_{\text{SN}}, y_{\text{SN}}), \quad (7)$$

where  $(x_{\text{SN}}, y_{\text{SN}})$  are the coordinates of the SNIa in each host galaxy image, converted from standard RA/DEC coordinates with the *AstroPy* library for Python (Astropy Collaboration et al. 2013) which includes World Coordinate System (WCS) transformation functions (Calabretta & Greisen 2002). This is the distance between an SNIa and its host galaxy if the SNIa were moved along an isophote contour to line up with the semi-major axis of the host. The galactocentric distance would then be obtained by dividing this distance by the scale length,  $r_e$ :

$$d_r \equiv \frac{r_{\text{SN}}}{r_e}, \quad (8)$$



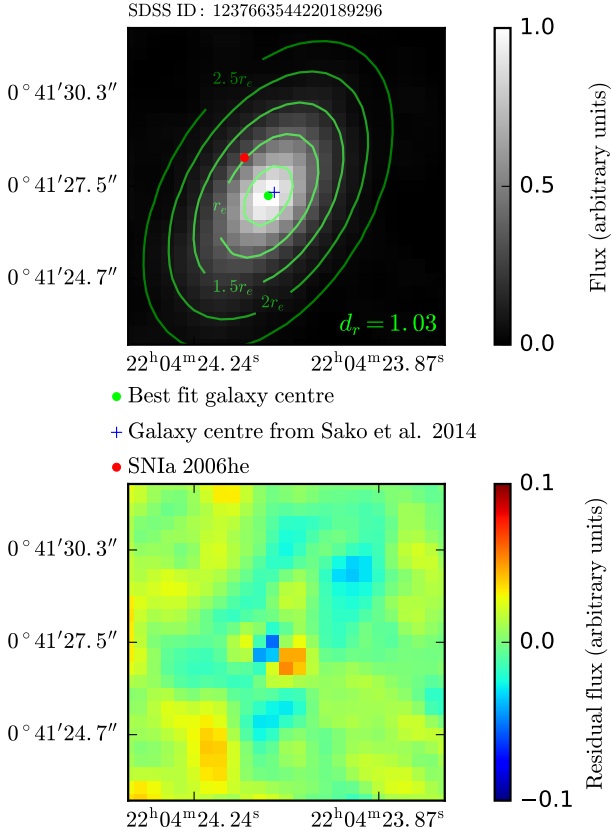


**Figure 2.** Top: *IMFIT* contours of the MLE fit for the galaxy shown in Fig. 1. Green lines indicate isophote contours from our model, with  $r_e$  the scale length of the radial intensity profile, Eq. (1). The green dot indicates the MLE for the centre of the galaxy, the blue cross indicates the centre of the galaxy reported in the SDSS-II Supernova Survey (Sako et al. 2014) and the red point indicates the location of SNIa 2006he. In this case  $d_r = 1.03$ . Bottom: Residuals between our best-fit galaxy optical emission model from the data.

This definition of the impact parameter is a good description of the SNIa – host galaxy distance as it takes into account the geometry of the light distribution of the host galaxy, which we are taking to be a proxy for dust and the main contributor to SNIAs extinction.

Notice that the galactocentric distance defined in Eq. (8) is normalized to the scale length  $r_e$ , rather than to the Petrosian half-light radius as in Sako et al. (2014). On average, our scale lengths are larger than the half-light radii scale lengths in Sako et al. (2014), which results in our values of  $d_r$  being on average smaller than what is reported in Sako et al. (2014). Nevertheless, the correlation coefficient between our galactocentric distance and the equivalent quantity in Sako et al. (2014) is 0.81.

A full analysis would also include an estimate of the uncertainty in  $d_r$  stemming from the fit to the galaxy image, uncertainty in the SNIa position and model uncertainty in choosing a parameterized model for the galaxy’s brightness. Although we ignore these uncertainties here, we highlight this as a point worth re-visiting in future work.

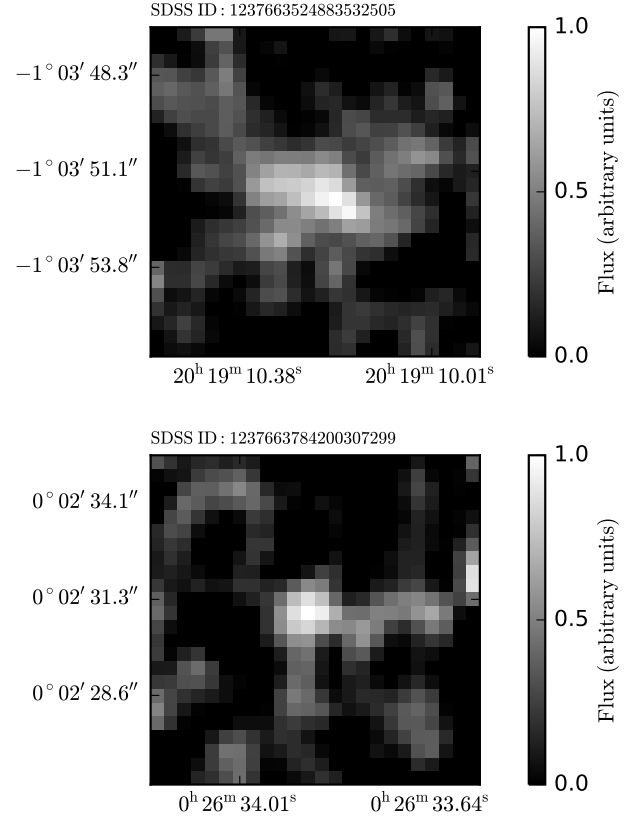


**Figure 3.** Top: an example of a galaxy image that is too faint to be fit with *IMFIT*. Bottom: an example of a galaxy image that is too noisy to be fit with *IMFIT*. SNIAs associated with galaxies that led to unsuccessful fits were not included in the analysis.

According to our hypothesis, SNIAs further from their galactic centre (i.e., with  $d_r \gg 1$ ) should explode in a galactic environment with a smaller dust column density, and hence they should exhibit less dust absorption. Following Anderson et al. (2015a), we also expect that SNIAs at large galactocentric distances ought to exhibit bluer values for the colour correction. We therefore expect the distribution of the colour correction parameter  $c$ , to differ for SNIAs with larger  $d_r$  than for those with  $d_r$  close to 0. In order to test this hypothesis, we split the sample of 280 SNIAs with  $d_r$  values into two groups, one with  $d_r < d_{\text{cut}}$  and the other with  $d_r \geq d_{\text{cut}}$ , where  $d_{\text{cut}}$  is a cut-off value.

The choice of  $d_{\text{cut}}$  is important in establishing the significance (or otherwise) of the effect of  $d_r$  on  $c$ . Given the distribution of  $d_r$  in our sample, shown in Fig. 4, a larger value of  $d_{\text{cut}}$  is expected to give a cleaner sample (i.e., SNIAs less affected by dust) but at the price of a very small sample size. On the other hand, choosing a smaller cut-off value  $d_{\text{cut}}$  may lead to a substantial number of SNIAs with  $d_r \geq d_{\text{cut}}$  that are still affected by dust. We chose a value of  $d_{\text{cut}} = 2$  for our analysis, as it is reasonable to assume a transition in the amount of dust at an galactocentric distance of about twice the value of the scale radius of the galaxy. We emphasize that we are not choosing the value of  $d_{\text{cut}}$  to maximize the significance of the effect. This means that our test statis-

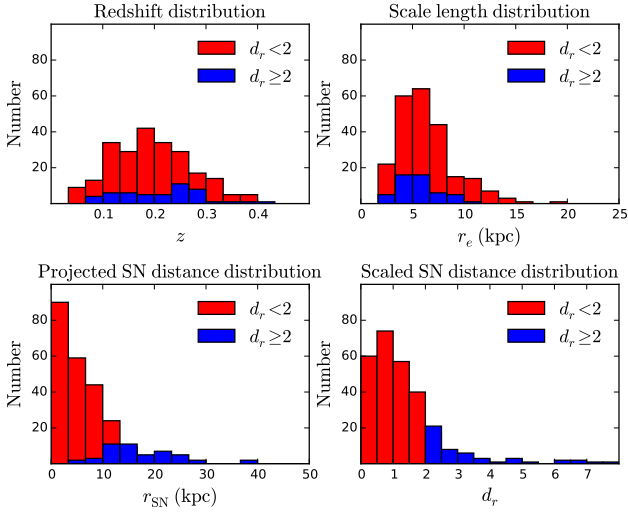


**Figure 4.** The distribution of SNIa redshifts, host galaxy scale radii  $r_e$ , projected galactocentric distance of SNIas,  $r_{\text{SN}}$ , and normalized galactocentric distances  $d_r$ . Here,  $r_e$  is the length of the semi major axis of an ellipse centred on a host galaxy which extends out to where the central intensity has fallen to a fraction  $e^{-b_n}$  of the central intensity.  $d_r$  is computed as the distance between a SNIa and the centre of its host galaxy if the SNIa were moved along a line of constant intensity to line up with the semi-major axis of the host, expressed in units of  $r_e$ .

tics does not need to be corrected for multiple testing (i.e., there is no “look elsewhere effect”). However, we do, *a posteriori* check the significance of our results as a function of  $d_{\text{cut}}$ , as described below.

Using the fixed choice of  $d_{\text{cut}} = 2$ , we define two groups of SNIas, (i) those with  $d_r < 2$  (231 SNIas) and (ii) those with  $d_r \geq 2$  (49 SNIas). The distributions of stretch and colour for the two groups are shown in Fig. 5. The stretch distributions for the two groups are similar, while the  $d_r \geq 2$  group appears bluer, i.e., there are more objects with  $c < 0$ .

We use a two-sample Kolmogorov-Smirnov (KS) test to assess the statistical significance of the difference in the colour distributions of the two groups. The KS test statistic is the maximum difference between the cumulative distribution function of two empirical distributions,  $D_{\text{max}}$ . Here we compare the cumulative distributions of the colour for the two groups of SNIas.  $D_{\text{max}}$  is compared to a threshold value

$$D_{n_1, n_2}(\alpha) = \kappa(\alpha) \sqrt{\frac{n_1 + n_2}{n_1 n_2}} \quad (9)$$

where  $\kappa(\alpha)$  is an  $\alpha$ -dependent critical value and  $n_1$  and  $n_2$  are the numbers of objects in each of the two groups. The test is significant (at the level  $\alpha$ ) if  $\Delta \equiv D_{\text{max}} - D_{n_1, n_2}(\alpha) > 0$ . For  $\alpha = 0.05$ , the critical level is  $\kappa(0.05) = 1.36$ .

To investigate the sensitivity of this result to the choice of  $d_{\text{cut}}$ , we evaluate  $\Delta$  as a function of  $d_{\text{cut}}$  for comparing the distributions of both the colour and stretch corrections in the two SNIa groups. With a significance level of  $\alpha = 0.05$ , the KS test for the stretch distribution is not significant for any value  $1 \leq d_{\text{cut}} \leq 2.5$ . (We do not consider larger values for  $d_{\text{cut}}$  as the number of SNIas in the  $d_r \geq d_{\text{cut}}$  group them

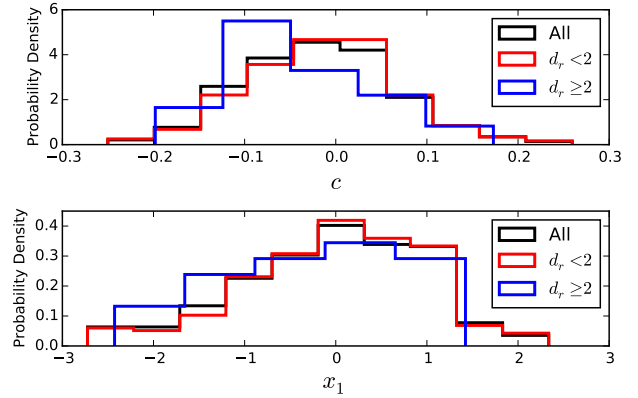


**Figure 5.** Histograms for the observed colour (top) and stretch (bottom) correction. Red is the  $d_r < 2$  sub-group, blue is for  $d_r \geq 2$ , black is for all SNIas combined. The distribution for colour with  $d_r \geq 2$  is bluer (i.e.,  $c < 0$ ). The distributions for stretch are similar for both sub-groups.

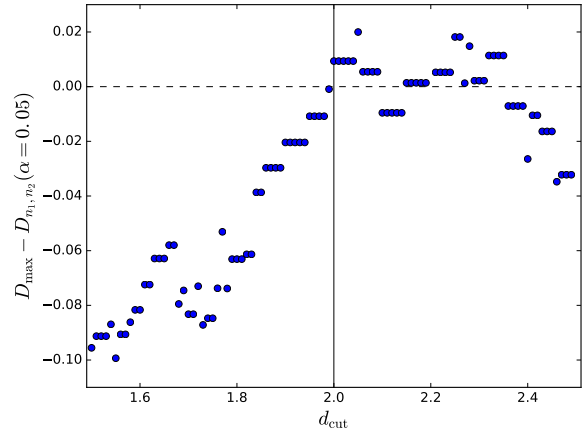


**Figure 6.** Difference between the KS test statistics and the  $\alpha = 0.05$  significance threshold as a function of the chosen cutoff value for the two SNIas groups. Our (fixed) choice,  $d_{\text{cut}} = 2$ , is indicated by the vertical black line. A value  $> 0$  (i.e., above the dashed horizontal line) indicates a statistically significant difference at the 5% level between the observed distributions of the colour correction in the two SNIa groups.

becomes too small.) The KS test is, however, statistically significant for the colour distribution for  $2.00 \leq d_{\text{cut}} \leq 2.09$  and for  $2.15 \leq d_{\text{cut}} \leq 2.35$ , as shown in Fig. 6. To avoid the statistical penalty for multiple testing, we do not choose the value of  $d_{\text{cut}}$  to achieve maximum significance, but rather carry out the KS test with a blind choice of  $d_{\text{cut}} = 2$ .

### 3 EVALUATING THE RESIDUAL SCATTER

After the empirical colour and stretch corrections, SNIas still exhibit a residual scatter in their (standardized) intrinsic magnitudes. Reducing this scatter enables more precise

estimation of the cosmological parameters, since it allows for a more precise measurement of the distance modulus as a function of redshift. Here we turn to the question of whether there is a statistically significant difference between the magnitude of the residual scatter in the two subgroups defined in Section 2.3. We use the Bayesian hierarchical framework *BAHAMAS* (March et al. 2011; Shariff et al. 2016) to estimate the residual scatter of the two groups. This fully Bayesian approach is different from the classical  $\chi^2$  approach in two fundamental ways.

Firstly, for each observed variable a latent (true) unobserved value is introduced using a hierarchical representation of the probabilistic relationships between the latent variables, observations and population parameters. More specifically,

$$m_{Bi}^* = \mu_i(\hat{z}_i, \mathcal{C}) - \alpha x_{1i} + \beta c_i + M_i^\epsilon. \quad (10)$$

encapsulates the linear corrections to the B-band peak apparent magnitude,  $m_{Bi}^*$ , captured by the SALT2 correction, namely  $c_i$  (colour) and  $x_{1i}$  (stretch). Here,  $\mu_i(\hat{z}_i, \mathcal{C})$  is the distance modulus, which depends on the SN's redshift,  $\hat{z}_i$ , and the underlying cosmological parameters,  $\mathcal{C}$ ;  $\{\alpha, \beta\}$  are regression coefficients to be estimated, and  $M_i^\epsilon$  is the residual absolute magnitude after empirical corrections. More specifically, the SALT2 colour parameter is defined as  $c = (B - V)_{\max} - \langle (B - V)_{\max} \rangle$ , where all colours are evaluated at the time of B-band maximum and  $\langle (B - V)_{\max} \rangle$  is the colour averaged over the SNIas in the templates (Guy et al. 2007). A value of  $c < 0$  means that the blue band magnitude is smaller (i.e., brighter) than the V band, hence the object is bluer. On the other hand,  $c > 0$  means the object is redder (than average). Unlike in the  $\chi^2$  approach, in *BAHAMAS*  $\{m_{Bi}^*, x_{1i}, c_i\}$  are latent variables that are stochastically related to their observed counterparts, but differ from the data because of observational noise. Since the SNIas in our data are spectroscopically confirmed, the errors in redshift can be ignored. The redshift range of the SNIas used in this analysis is restricted by the need to acquire host galaxy images, and spans  $0.04 < z < 0.40$ . With this narrow range, SNIa data alone cannot constrain the cosmological parameters. We therefore assume a flat  $\Lambda$ CDM universe with a fixed cosmology,  $\{\Omega_m = 0.315, H_0 = 67.3\}$ , matching the posterior mean value obtained by the *Planck* Cosmic Microwave Background mission (Planck Collaboration et al. 2015).

The second key feature of the Bayesian approach is its ability to account for population variability. Instead of assuming that each SNIa has the same absolute magnitude (after corrections), we assume that they vary probabilistically with an underlying population-level distribution. Specifically, we model the residual absolute magnitude,  $M_i^\epsilon$ , using a Gaussian distribution:

$$M_i^\epsilon \sim \mathcal{N}(M_0, \sigma_{\text{res}}^2), \quad (11)$$

where  $M_0$  is the mean of the residual absolute magnitudes and  $\sigma_{\text{res}}$  is its residual standard deviation, quantifying the residual scatter of SNIas after corrections. This quantity is to be understood as a phenomenological error describing the intrinsic residual variability that is not accounted for by the empirical corrections for stretch and colour.

It was demonstrated by March et al. (2011) with simulated data that (a precursor of) the Bayesian approach used

in *BAHAMAS* results in less biased, more accurate estimates than the standard  $\chi^2$  approach, while improving overall coverage of the ensuing credible intervals. We apply *BAHAMAS* to the two SNIa groups ( $d_r < 2$  and  $d_r \geq 2$ ), as well as to the whole dataset for comparison, and obtain the marginal posterior distribution of  $\{\alpha, \beta, \sigma_{\text{res}}\}$  numerically using the sampler presented in Shariff et al. (2016). Full details of *BAHAMAS*, including prior choices, hierarchical structure and the sampling algorithms are given in Shariff et al. (2016).

Our approach to estimating the residual scatter, and the colour and stretch corrections parameters is significantly more sophisticated than what has been adopted in previous works attempting to establish the influence of galactocentric distance (Ivanov et al. 2000; Galbany et al. 2012). The Bayesian method adopted here has the advantage of exploiting the probabilistic nature of the model to ‘borrow strength’ between SNIae, thus increasing sensitivity to subtler features in the data than relative to the cruder  $\chi^2$  approach. Furthermore, we produce a full marginal probability distribution for the value of the intrinsic scatter, not just a point estimate. As shown in March et al. (2011) this results in more accurate and precise estimates for the parameters of interest than it is possible with the standard  $\chi^2$  method.

In the present work we segregate SNIas according to the two sub-groups defined above. Alternatively, one could include  $d_r$  as an additional linear covariate in the correction term in Eq. (10), the slope of which would be another free parameter, thus replacing Eq. (10) with:

$$m_{Bi}^* = \mu_i(\hat{z}_i, \mathcal{C}) + X_i^T \mathcal{B} + M_i^\epsilon, \quad (12)$$

where  $X_i = \{x_{1i}, c_i, d_{r,i}\}^T$  and  $\mathcal{B} = \{-\alpha, \beta, \gamma\}^T$ , with  $\gamma$  the slope of the galactocentric distance covariate. One would then fit the value of  $\gamma$  together with the colour and stretch correction coefficients,  $\alpha$  and  $\beta$ . The inclusion of galactocentric distance as an additional standardization variable is akin to how the host galaxy mass correction is usually parameterized. In both cases, one can either segregate the SNIas in two groups, divided by a cutoff value, or use the additional covariate as a linear correction term in the distance modulus, as was done e.g., in Shariff et al. (2016). The second approach dispenses with the need of defining an arbitrary cutoff point.

In previous studies, Ivanov et al. (2000); Galbany et al. (2012) investigated the impact of galactocentric distance as a covariate. Galbany et al. (2012) also used only two bins (‘near’ and ‘far’). Importantly, the ‘near’ and ‘far’ bins were defined by splitting the SNIas into two groups of equal size (and further subdividing them according to host morphology), and not with reference to their normalized galactocentric distance, like we do here. This might have washed out any potential correlation. A puzzling result of Galbany et al. (2012) is that while  $c$  decreased with distance (with a reported significance of the correlation coefficient of  $4.4\sigma$ ) for the entire data set, the effect disappeared when the data were split according to morphology. Yasuda & Fukugita (2010) also adopted (de-projected) galactocentric distance as a covariate, finding no effect. They, however, did not attempt to normalize the galactocentric distance to the host light radius, as we do here.

For simplicity, we only consider splitting the SNIas into two groups (with a hard, pre-defined cut), and leave inves-

tigation of the galactocentric distance as a linear covariate to future work.

#### 4 RESULTS

The marginal posterior distributions in one and two dimensions for the parameters of interest,  $\{\alpha, \beta, \sigma_{\text{res}}, M_0^\epsilon\}$  are shown in Fig. 7, split according to sub-group and compared with the result for the whole data set. Table 1 gives posterior summary statistics for the same quantities. In both cases, the latent parameters  $\{c_i, x_{1,i}, m_{B,i}^*\}$  ( $i = 1, \dots, N$ , where  $N = 280$  is the number of SNIas considered) and all other population-level parameters,  $\{c_*, R_c, x_*, R_x\}$ , have been marginalized out. Here,  $c_*$  and  $x_*$  are the (redshift-independent) population means of the colour and stretch distributions, respectively, and  $R_c, R_x$  are their variances. These distributions are taken to be Gaussian, see Shariff et al. (2016) for full details.

We observe shifts in the distributions of the all quantities except for  $M_0^\epsilon$  for the two different sub-groups. The most dramatic difference is in the value of the residual scatter,  $\sigma_{\text{res}}$ . Its posterior distribution is fairly Gaussian, and has posterior average and standard deviation given by  $\sigma_{\text{res}} = 0.106 \pm 0.009$  for the  $d_r < 2$  sub-group, which is reduced to  $\sigma_{\text{res}} = 0.074 \pm 0.021$  for the  $d_r \geq 2$  sub-group. This represents a reduction of  $\approx 30\%$  in the posterior mean values. The significance of the difference is approximately  $1.4\sigma$  (computed using the standard deviation of the difference between  $\sigma_{\text{res}}$  in the two subgroups and assuming Gaussian errors). While this is not strongly significant, we emphasize the small sample size ( $N_{\text{SNIa}} = 49$  for the  $d_r \geq 2$  sub-group), which results in a fairly wide posterior distribution for  $\sigma_{\text{res}}$ . This means that SNIas at large galactocentric distances show better standardization properties (i.e., are more uniform in their magnitudes after corrections) than the whole data set. This is additionally supported by Fig. 8, showing the Hubble residuals of the two sub-groups. The right/red ( $d_r \geq 2$ ) residuals are clearly smaller than the left/blue ones ( $d_r < 2$ ). SNIas further away from the centre of the galaxy have, on average, smaller residuals after corrections. Therefore, cosmological distance estimation from this sub-group can be expected to be more precise.

We show in Figures 9 and 10 the inferred posterior mean and standard deviation for the latent colour and (post-correction) intrinsic magnitude for each SNIa, fit separately for the two subgroups. Fig. 9 shows that indeed the  $d_r \geq 2$  sub-group has a latent colour distribution that is skewed towards bluer objects. From Fig. 10 we observe that the  $d_r \geq 2$  sub-group distribution of intrinsic magnitudes is tighter. Also, the population averages for the two sub-groups (represented by horizontal dashed lines) are indistinguishable. This means that we do not find any evidence for intrinsic differences in the average, post-correction magnitudes in the SNIas in the two sub-groups.

One could imagine that the explanation for this effect might lie in the reduced amount of dust found at high galactocentric radii: since the observed colour variation is the sum of intrinsic colour variability and reddening due to the host galaxy and/or local circumstellar material (CSM) dust (which varies from host to host), reducing the host galaxy colour variability should lead to a smaller residual scatter

after correction, as observed in our findings. However, this interpretation is at odds with the results for the value of the colour correction coefficient,  $\beta$ . While differences in the posteriors for  $\alpha$  and  $\beta$  between the two sub-groups are less pronounced, we do observe a (very modest) shift to larger values of both  $\alpha$  and  $\beta$  for the  $d_r \geq 2$  sub-group. Of particular interest for our discussion is the value of the colour correction parameter,  $\beta$ .

There is evidence (Wang 2005; Goobar 2008) that the local CSM might have smaller size dust grains (compared to the Milky Way), leading to a smaller value of the total-to-selective extinction  $R_V \equiv A_V/E(B-V)$  than the average Milky Way value of  $R_V^{\text{MW}} = 3.1$ . Here,  $A_X$  is the extinction (in mag) in band  $X$ , i.e.,  $A_X = m_X - m_{X,0}$ , where  $m_X$  is the apparent magnitude in band  $X$  and  $m_{X,0}$  is the apparent magnitude in the same band in the absence of extinction. The colour excess  $E(B-V)$  is given by  $E(B-V) = (m_B - m_V) - (m_{B,0} - m_{V,0}) = A_B - A_V$ . Given that total extinction and reddening is the cumulative effect of local CSM dust and ISM dust, if the effect of the ISM were largely removed by the cut to large  $d_r$ , one would expect this sub-group to exhibit the reddening law of the underlying CSM, which is typically steeper<sup>1</sup> than the Milky Way value. For example, for SN2014J Yang et al. (2016) found evidence of a luminous arc – attributed to the CSM – with an estimated  $R_V^{\text{CSM}} \approx 1.4$ . Recall that, from Eq. (10),  $\beta$  is the slope that gives the change in  $B$  band magnitude for a unit change in the value of  $B-V$ . Therefore,  $\beta$  ought to be compared to  $R_B \equiv A_B/E(B-V)$ . Given their respective definitions, it follows that  $R_B - R_V = (A_B - A_V)/E(B-V) = 1$ , hence  $R_B = R_V + 1$ . From this, one would expect that reddening due to the CSM should typically show  $\beta^{\text{CSM}} = R_V^{\text{CSM}} + 1 \approx 2.4$ , i.e., a much smaller value than we observe in the  $d_r \geq 2$  sub-sample, for which  $\beta = 3.44 \pm 0.36$ .

Alternatively, in the absence of CSM reddening one would expect the inferred value of  $\beta$  for the  $d_r \geq 2$  sub-sample to recover the value associated with the intrinsic colour variability of the SNIas. This has been estimated by Mandel et al. (2016) in a low-redshift sample, finding  $\beta^{\text{int}} = 2.210 \pm 0.255$ , again much lower than the value we obtain for our sub-sample at high galactocentric distance. Mandel et al. (2016) argue that the simple linear colour correction formula (which we adopt in this work, in line with standard usage) effectively averages between the intrinsic colour correction,  $\beta^{\text{int}}$ , and the reddening law slope. Thus one would expect that if indeed the  $d_r \geq 2$  sub-group had negligible reddening due to the ISM, we would observe a value of  $\beta$  that averages between the  $\beta^{\text{int}} = 2.210$  value found by Mandel et al. (2016) and the CSM reddening law, equivalent to  $\beta \approx 2.2 - 2.4$ . Thus the inferred  $\beta$  for the  $d_r \geq 2$  sub-group ought to be around 2.2, which is not what we observe.

Folatelli et al. (2010) analysed the first set of low-redshift SNIas from the Carnegie Supernovae Project (CSP), and found  $R_V \approx 1.7$  ( $\beta \approx 2.7$ ) for the entire set of SNIas. However, when excluding two highly reddened SNIas from

<sup>1</sup> The wavelength dependency of extinction in the vicinity of the  $V$  band is approximately linear in  $1/\lambda$  with slope  $1/R_V$ , where  $\lambda$  is the wavelength (Cardelli et al. 1989). Hence a smaller value of  $R_V$  results in a steeper reddening law.



	$d_r < 2$	$d_r \geq 2$	All data
$\alpha$	$0.134 \pm 0.012$	$0.173 \pm 0.020$	$0.144 \pm 0.040$
$\beta$	$3.079 \pm 0.162$	$3.445 \pm 0.357$	$3.068 \pm 0.145$
$M_0^\epsilon$	$-19.1804 \pm 0.0262$	$-19.1735 \pm 0.0357$	$-19.1782 \pm 0.0242$
$\sigma_{\text{res}}$	$0.106 \pm 0.009$	$0.074 \pm 0.021$	$0.105 \pm 0.008$

**Table 1.** Marginal posterior average and standard deviation for the stretch,  $\alpha$  and colour,  $\beta$ , correction parameters, as well as for the SNIas residual scatter  $\sigma_{\text{res}}$  (after empirical corrections) for the three cases considered: including only SNIas with small galactocentric distance ( $d_r < 2$ ), only SNIas with large galactocentric distance ( $d_r \geq 2$ ) and including all SNIas irrespective of galactocentric distance (‘All data’).

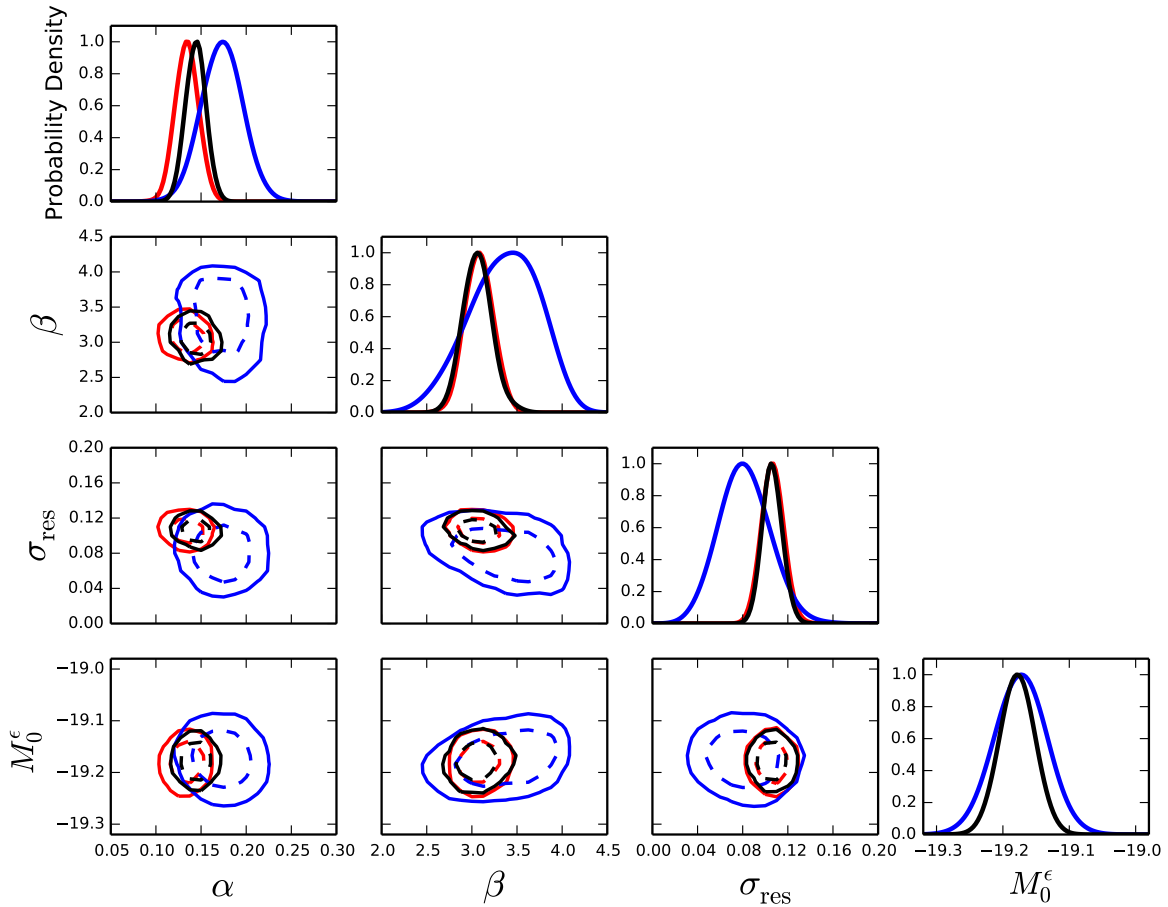


**Figure 7.** 1D and 2D marginal posterior distributions for  $\alpha$ ,  $\beta$ ,  $M_0^\epsilon$  (the average post-correction intrinsic magnitude) and  $\sigma_{\text{res}}$  (the residual scatter in the intrinsic magnitude), with all latent variables and other population-level parameters marginalized over. Red is for the sub-group at small galactocentric distance,  $d_r < 2$  ( $N_{\text{SNIa}} = 231$ ), blue is for the group at high galactocentric distance,  $d_r \geq 2$  ( $N_{\text{SNIa}} = 49$ ), while black is all SNIas combined. 1D posterior densities have been normalized to the peak. 2D contours depict 68% and 95% credible regions.

their analysis, they obtained  $R_V \approx 3.2$  ( $\beta \approx 4.2$ ), similar to our higher value for the  $d_r \geq 2$  sub-group. More recently, Burns et al. (2014) used the late-time Lira (1996) law to select a low-reddening sample of 34 SNIas from the Carnegie Supernovae Project (CSP). Their approach circumvents the use of galactocentric distance, which can be expected to as-

sign to the  $d_r < 2$  sub-group SNIas that are low reddened but at small projected radii (i.e., in front of the host). Burns et al. (2014) then employed a Bayesian hierarchical model to reconstruct the reddening law of the host (under a number of priors). They found that objects with the least reddening ( $E(B - V)_{\text{host}} < 0.2$ ) have a reddening law compatible

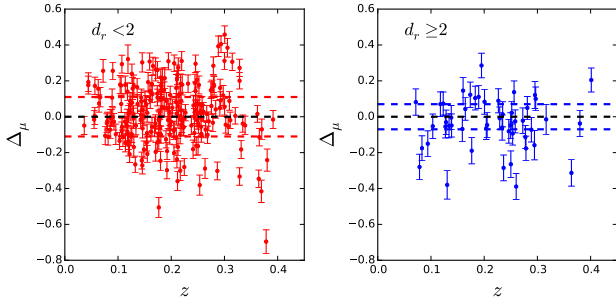


**Figure 8.** Hubble residuals as a function of redshift. The left panel shows the residuals for the SNIas with  $d_r < 2$ , while the right panel shows SNIas with  $d_r \geq 2$ . Error bars are the posterior standard deviation of the Hubble residual value. Also shown as horizontal dashed blue/red lines is the posterior mean of the residual scatter,  $\sigma_{\text{res}}$ , given in Table 1.

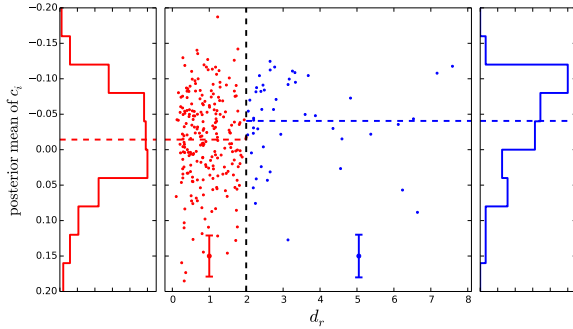


**Figure 9.** Posterior mean of the latent colour values (determined from our hierarchical model) as a function of galactocentric distance,  $d_r$ , colour coded according to the two sub-groups (split at  $d_r = 2$ ). The histograms at the margins show the 1D marginal distribution of latent colour values for the two subgroups. The  $d_r \geq 2$  sub-group clearly shows a preferentially bluer colour ( $c < 0$ ). The vertical errorbars give the average posterior standard deviation in the values of  $c_i$  for each of the two sub-groups.

with the Milky Way value of  $R_V = 3.1$  (corresponding to  $\beta = 4.1$ ). This is compatible with our observation of a shift of  $\beta$  to larger values in the  $d_r \geq 2$  group, which (being the bluer sub-group) exhibits the least reddening. This thus hints at the possibility that the shift of  $\beta$  to higher values for the  $d_r \geq 2$  sub-group is compatible with the hypothesis that the remaining reddening is due to the host ISM. Furthermore, despite not finding any correlation between colour and galactocentric distance, Yasuda & Fukugita (2010) do observe an excess of redder colour values at low galactocentric distances, compatible with the later findings of Anderson et al. (2015b). Another heuristic (if counterintuitive) argument in support of our findings comes from the fact that less massive galaxies (with stellar mass  $M_* < 10^{10} M_\odot$ ) show a larger value of  $\beta$  (Sullivan et al. 2010). These galaxies are also the ones with the least dusty environments (Garn & Best 2010). Hence a larger value of  $\beta$  can be associated with less dusty environments.

Taken all together, the above arguments lend credence

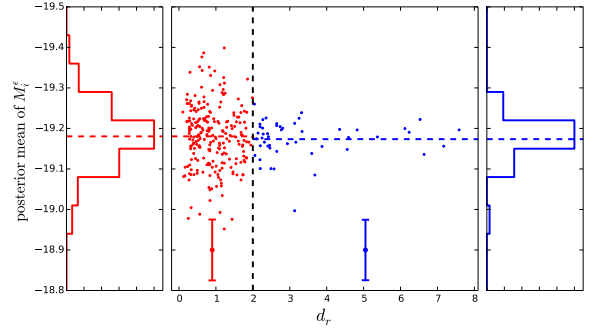


**Figure 10.** Posterior mean of the (post-correction) intrinsic magnitude for the two sub-groups. SNIas at large galactocentric distance ( $d_r \geq 2$ ) exhibit a tighter distribution around the mean magnitude. The vertical errorbars give the average posterior standard deviation in the values of  $M_i^c$  for each of the two sub-groups.

to the hypothesis that the large  $d_r$  sub-group is actually probing a low-reddening/low-attenuation ISM environment, rather than seeing the underlying CSM/intrinsic colour scatter. The reduction in residual intrinsic scatter we observe could be the resultant of the  $d_r \geq 2$  sub-group being subject to a less dusty ISM, as well as to the more homogeneous metallicity and SFR environment for this sub-group. Further work is required to disentangle the physical origin of this effect, and we comment on this aspect in the next section.

In this work we have not divided hosts in terms of their morphology. Since early-type galaxies are dominated by old stars and relatively dust-free (Wise & Silva 1996), while spirals have star-forming activity in the arms and a diverse (age-wise) stellar population, SNIas that occur in early-type galaxies are less likely to be significantly affected by dust. In spirals, central stars tend to be both older and metal rich than in outer regions, and therefore classifying SNIas according to both radial distance and galaxy type could potentially disentangle the effects due to stellar age and metallicity from those due to dust properties. One might therefore speculate that including host galaxy morphology information could help in further reducing the residual scatter, and perhaps in clarifying the origins of the effect. Lampeitl et al. (2010) subdivided the SDSS-II SNIa sample in two groups, according to the passive or star forming nature of their host galaxies (based on their estimated SFR). They found a strong difference in the stretch parameter,  $x_1$ , for the two groups, but no significant difference in the colour, concluding that SNIas must have the same intrinsic colour variations in all galaxy types. This conclusion was confirmed by Henne et al. (2017), who examined the influence of galaxy morphology by classifying hosts in three groups – ellipticals/lenticulars (E,S0), early-type spirals (Sa-Sc), late-type spirals (Sd-Ir) – for 192 SNIas from JLA. While they reported  $1\sigma$  shifts in the reconstructed values of  $\alpha, \beta$  depending on galactic morphology group, they did not find any significant correlation between colour and host morphology. This conclusion stood despite a weak trend of slightly bluer colour SNIas in early type (i.e., passive) hosts. This was interpreted as being due to the larger amount of dust in spirals, which would thus make the SN colour redder. The above studies thus seem to

suggest that our results are not strongly affected by the lack of morphological host information.

This work does not consider colour-based selection effects over and above the (magnitude) corrections already implemented in the JLA sample. There is evidence that high- $z$  SNIa are bluer (Rubin & Hayden 2016) and come from less dusty environment (Mandel et al. 2016) due to selection bias. However, our  $d_r \geq 2$  sub-group spans almost the entire SDSS-SNIa redshift range (see Fig. 4), with the majority of the SNIas at  $z < 0.3$ , and hence colour-based selection effects are unlikely to be playing a major role here.

## 5 CONCLUSIONS

We have measured the projected galactocentric distance to the host of the SNIas for a sub-set of the SDSS Type Ia SNIas in the JLA sample and investigated the scatter around the Hubble diagram (for a fixed cosmology) for two sub-groups, separated by a cut in their distance. The rationale was that SNIas at large galactocentric distances might be less subject to ISM reddening and absorption, and might explode in more homogeneous environments in terms of metallicity and local SFR.

We have demonstrated that SNIas further away from the host can be standardized to a higher degree, in that their intrinsic dispersion (post Phillips corrections) is reduced from  $\sigma_{\text{res}} = 0.105 \pm 0.008$  (for the full sample) to  $\sigma_{\text{res}} = 0.074 \pm 0.021$  (for the SNIas with larger galactocentric distances). The statistical significance of the effect is, however, small (about  $1.4\sigma$ ). This is primarily due to the smallness of the sample (only 42 SNIas in the  $d_r \geq 2$  sub-group). Future surveys and data tabulations should be encouraged to include measured galactocentric distances (and, perhaps, morphology of host) to account for this effect. In a Bayesian framework, it would be straightforward to include prior information on extinction and reddening depending on galactocentric distance and morphology of host. This has the potential to improve accuracy and precision for inferred cosmological parameters.

Future work should focus on verifying whether a larger sample size can confirm this tentative result. The SDSS-II SN sample contains a larger number of photometrically observed SNIa, which have not been included in this analysis. Campbell et al. (2016) analysed 721 SNIas from this larger data set, and used different host properties such as age and metallicity to reduce the Hubble residual. Given the availability of SDSS imagery for the hosts, the additional supernovae in the photometric SDSS sample could be analyzed to corroborate or disprove this result. Since this is a photometric sample, there is a possibility of contamination of the sample by non-SNIa's. A Bayesian supernova classifier (Hlozek et al. 2012; Jones et al. 2016; Revsbech et al. 2017) can be used to account for this. Additionally, since this photometric sample contain SNIa to a higher redshift, selection effects may play a major role and have to be correctly accounted for (e.g. as in Rubin et al. (2015)). Another, complementary low-redshift ( $0.01 < z < 0.10$ ) SNIas sample is the one used in Mandel et al. (2016), from a compilation of data including high-quality light curves from the CfA and CSP surveys. An advantage of this lower redshift data set is that detailed morphological studies can be carried

out on these relatively nearby galaxies, to verify whether or not host galaxy type plays a role in the correction procedure. Furthermore, the source of the difference in  $\beta$  value from the two sub-groups could be elucidated by analyzing them with the SIMPLE-BayesSN framework (Mandel et al. 2016). The upcoming SNIa data from the Dark Energy Survey (expected to be released in 2017) would also be a very useful testing ground for our method. We leave exploration of all these avenues to future work.

*Acknowledgements:* we thank Heather Campbell, Kaisey Mandel and Marc Sullivan for useful discussions. This work was supported by Grant ST/N000838/1 from the Science and Technology Facilities Council (UK). RT was partially supported by an EPSRC ‘‘Pathways to Impact’’ grant. DvD was supported by a Wolfson Research Merit Award (WM110023) provided by the British Royal Society and by Marie-Curie Career Integration (FP7-PEOPLE-2012-CIG-321865) grant provided by the European Commission. RT, DvD and HS were supported by a Marie-Skodowska-Curie RISE (H2020-MSCA-RISE-2015-691164) Grant provided by the European Commission.

## REFERENCES

- Ahn C. P., et al., 2014, *Astrophysical Journal Supplement*, 211, 17
- Amanullah R., et al., 2010, *Astrophys. J.*, **716**, 712
- Anderson J. P., James P. A., Haberman S. M., Galbany L., Kuncarayakti H., 2015a, *Publ. Astron. Soc. Austral.*, 32, 19
- Anderson J. P., James P. A., F  rster F., Gonz  lez-Gait  n S., Haberman S. M., Hamuy M., Lyman J. D., 2015b, *Mon. Not. Roy. Astron. Soc.*, 448, 732
- Astier P., et al., 2006, *Astron. Astrophys.*, 447, 31
- Astropy Collaboration et al., 2013, *Astronomy and Astrophysics*, 558, A33
- Bailey S., et al., 2008, arXiv:0810.3499,
- Balland C., et al., 2009, *Astronomy & Astrophysics*, **507**, 85
- Betoule M., et al., 2014a, *Astron. Astrophys.*
- Betoule M., et al., 2014b, *Astronomy and Astrophysics*, 568, A22
- Burns C. R., et al., 2014, *ApJ*, **789**, 32
- Calabretta M. R., Greisen E. W., 2002, *Astronomy and Astrophysics*, 395, 1077
- Campbell H., et al., 2013, *ApJ*, **763**, 88
- Campbell H., Fraser M., Gilmore G., 2015, *MNRAS*
- Campbell H., Fraser M., Gilmore G., 2016, *MNRAS*, **457**, 3470
- Cardelli J. A., Clayton G. C., Mathis J. S., 1989, *Astrophys. J.*, 345, 245
- Ciotti L., Bertin G., 1999, *Astronomy and Astrophysics*, 352, 447
- Contreras C., et al., 2010, *Astrophys. J.*, **139**, 519
- D’Andrea C. B., et al., 2011, *ApJ*, **743**, 172
- Doi M., et al., 2010, *Astronomical Journal*, 139, 1628
- Erwin P., 2015, *Astrophysical Journal*, 799, 226
- Folatelli G., et al., 2010, *AJ*, **139**, 120
- Freedman W. L., Burns C. R., Phillips M., Wyatt P., Persson S., et al., 2009, *Astrophys. J.*, 704, 1036
- Galbany L., et al., 2012, *Astrophysical Journal*, 755, 125
- Gallagher J. S., Garnavich P. M., Caldwell N., Kirshner R. P., Jha S. W., Li W., Ganeshalingam M., Filippenko A. V., 2008, *Astrophys. J.*, 685, 752
- Garn T., Best P., 2010, *Mon. Not. Roy. Astron. Soc.*, 409, 421
- Goobar A., 2008, *Astrophys. J.*, 686, L103
- Guy J., et al., 2007, *Astron. Astrophys.*, 466, 11
- Henne V., et al., 2017, *New Astron.*, 51, 43
- Hicken M., et al., 2009, *Astrophys. J.*, 700, 331
- Hlozek R., et al., 2012, *ApJ*, **752**, 79

- Ivanov V. D., Hamuy M., Pinto P. A., 2000, *Astrophysical Journal*, 542, 588
- Jha S., Riess A. G., Kirshner R. P., 2007, *Astrophys. J.*, 659, 122
- Jones D. O., Riess A. G., Scolnic D. M., 2015, *Astrophys. J.*, 812, 31
- Jones D. O., et al., 2016, 1611.07042
- Kasen D., Woosley S. E., 2007, *Astrophys. J.*, 656, 661
- Kelly P. L., Hicken M., Burke D. L., Mandel K. S., Kirshner R. P., 2010, *Astrophys. J.*, 715, 743
- Kelly P. L., Filippenko A. V., Burke D. L., Hicken M., Ganeshalingam M., Zheng W., 2015, *Science*, 347, 1459
- Kessler R., et al., 2009, *Astrophys. J. S.*, 185, 32
- Kowalski M., et al., 2008, *Astrophys. J.*, 686, 749
- Lampeitl H., et al., 2010, *Astrophysical Journal*, 722, 566
- Lira P., 1996, Master's thesis, MS thesis. Univ. Chile (1996)
- MacArthur L. A., Courteau S., Holtzman J. A., 2003, *Astrophysical Journal*, 582, 689
- Maeda K., Terada Y., 2016, *Int. J. Mod. Phys.*, D25, 1630024
- Mandel K. S., Wood-Vasey W. M., Friedman A. S., Kirshner R. P., 2009, *ApJ*, 704, 629
- Mandel K. S., Scolnic D., Shariff H., Foley R. J., Kirshner R. P., 2016, preprint ([arXiv:1609.04470](https://arxiv.org/abs/1609.04470))
- March M. C., Trotta R., Berkes P., Starkman G. D., Vaudrevange P. M., 2011, *MNRAS*, 418, 2308
- Perlmutter S., et al., 1999, *Astrophys. J.*, 517, 565
- Phillips M., 1993, *Astrophys. J.*, 413, L105
- Phillips M. M., Lira P., Suntzeff N. B., Schommer R. A., Hamuy M., Maza J., 1999, *AJ*, 118, 1766
- Planck Collaboration et al., 2015, preprint,
- Rest A., Scolnic D., Foley R., Huber M., Chornock R., et al., 2014, *Astrophys. J.*, 795, 44
- Revsbech E., Trotta R., van Dyk D., 2017, To appear
- Riess A. G., Press W. H., Kirshner R. P., 1996, *Astrophys. J.*, 473, 88
- Riess A. G., et al., 1998, *Astron. J.*, 116, 1009
- Rigault M., et al., 2013, *Astron. Astrophys.*, 560, A66
- Rubin D., Hayden B., 2016, 1610.08972
- Rubin D., et al., 2015, *ApJ*, 813, 137
- Sako M., et al., 2014, preprint
- Scovaccicchi D., Nichol R. C., Macaulay E., Bacon D., 2016, arxiv: 1611.01315
- Sérsic J. L., 1963, *Boletín de la Asociación Argentina de Astronomía La Plata Argentina*, 6, 41
- Shariff H., Jiao X., Trotta R., van Dyk D. A., 2016, *The Astrophysical Journal*, 827, 1
- Sternberg A., et al., 2011, *Science*, 333, 856
- Sullivan M., et al., 2006, *Astrophys. J.*, 648, 868
- Sullivan M., et al., 2010, *Mon. Not. Roy. Astron. Soc.*, 406, 782
- Suzuki N., et al., 2012, *ApJ*, 746, 85
- Wang L., 2005, *Astrophys. J.*, 635, L33
- Wise M. W., Silva D. R., 1996, *ApJ*, 461, 155
- Wood-Vasey W. M., Miknaitis G., Stubbs C. W., 2007, *Astrophys. J.*, 666, 694
- Yang Y., et al., 2016, preprint ([arXiv:1610.02458](https://arxiv.org/abs/1610.02458))
- Yasuda N., Fukugita M., 2010, *Astron. J.*, 139, 39

This paper has been typeset from a  $\text{\TeX}/\text{\LaTeX}$  file prepared by the author.